J Comput Aided Mol Des (2012) 26:865–881
DOI 10.1007/s10822-012-9581-y

Understanding the molecular interactions of different radical scavengers with ribonucleotide reductase M2 (hRRM2) domain: opening the gates and gaining access

Arijit Basu · Barij N. Sinha

Received: 4 March 2012 / Accepted: 9 May 2012 / Published online: 26 May 2012

Abstract We employed a combination of molecular docking and dynamics to understand the interaction of three different radical scavengers (SB-HSC21, ABNM13 and trimidox) with ribonucleotide reductase M2 (hRRM2) domain. On the basis of the observed results, we can propose how these ligands interact with the enzyme, and cease the radical transfer step from the di-iron center to TYR176. All the ligands alter the electron density over TYR176, –OH group by forming an extremely stable H-bond with either –NHOH group, or with phenolic hydroxyl group of the ligands. This change in electronic density disrupts the water bridge between TYR176, –OH and the di-iron center, which stops the single electron transfer process from TYR176, –OH to iron. As a consequence the enzyme is inhibited. Another interesting observation that we are reporting is the two stage gate keeping mechanism of the RR active site tunnel. We describe these as the outer Gate-1 controlled by ARG330, and the inner Gate-2 controlled by SER263, PHE240, and PHE236. We also observed a dynamic conformational shift in these residues, the incoming ligands can go through, and interact with the underlying TYR176, –OH group. From the study we found the active—site of hRRM2 is extremely flexible and shows a significant induced fit.

Keywords Molecular dynamics · Ribonucleotide reductase (RR) · Gate keeper residues · Molecular docking

Electronic supplementary material The online version of this article (doi:10.1007/s10822-012-9581-y) contains supplementary material, which is available to authorized users.

A. Basu (✉) · B. N. Sinha
Department of Pharmaceutical Sciences, Birla Institute of Technology, Mesra, Ranchi 835 215, Jharkhand, India
e-mail: arijit4uin@gmail.com; abasu@bitmesra.ac.in

Introduction

Ribonucleotide reductase (RR) catalyzes the reduction of ribonucleotides to their corresponding deoxyribonucleotides, the building blocks for DNA in all living cells [1, 2]. There are three main classes (I, II and III) of RR, based on different metal cofactors for their catalytic activity [3–7]. Class I enzymes are found in all eukaryotic organisms yeast, algae, plants, and mammals. It is also expressed in some prokaryotes and viruses. Class I is further divided into three subclasses (Ia, Ib, and Ic) based on polypeptide sequence homologies and their overall allosteric regulation behavior [8, 9]. Human RR belongs to Class Ia. Reduction of ribonucleotides to deoxyribonucleotides is the rate-limiting step for DNA synthesis. Therefore, inactivation of RR stops DNA synthesis, as a consequence inhibits cell proliferation. The role of RR in DNA synthesis and repair is very important; this has made it an important target for anticancer drug design [10–12]. Many RR inhibitors are in clinical use, undergoing clinical trials, or have shown promising results in pre-clinical studies.

Structurally, RR is a tetrameric holoenzyme [1], made up of two homodimeric subunits, ($\alpha 2\beta 2$). The large $\alpha 2$-homodimer is called R1 (M1), and the small $\beta 2$-homodimer is called R2 (M2). M1 is the reductase component, which harbors the active site or the substrate binding site. This site participates in the catalytic reduction of ribonucleotides. The M2 site contains an oxygen-linked diferric iron center that generates a free radical (from TYR176 in human). Once the radical is generated, it is propagated by a relay mechanism to the catalytic active site of M1, which is separated by 35 Å from the di-iron center of M2. This is essential for nucleotide reduction process taking place at the substrate binding site in M1. The di-iron center of M2 can exist mainly in two different states. The diferrous

(Fe(II)Fe(II)) state, which spontaneously oxidize through a series of intermediate states, leading to a μ-oxo-bridged diferric (Fe(III)Fe(III)) state [13]. Molecules like hydroxyurea (HU), didox, trimidox, hydroxyguanidines (HG), hydroxamic acids, hydroxysemicarbazides (HSC) etc. were reported to interfere with the tyrosyl free-radical generation process, for inhibiting the enzyme RR. Mode of action of most of these analogs has been deduced either by cell line assays, or by spectroscopic studies, or by enzyme assays. No crystallographic information of the ligand bound M2 subunit has been reported till date. In absence of these information, structure based drug designing on this target is a concern, and yet to be explored. If we can develop a plausible model with a few inhibitors, it can easily serve as a reference point that can be used for future structure based drug designing.

As a starting point, for developing such kind of model, we scrutinized a few previously reported holo protein structures for human [14], mouse [15, 16], and *Escherichia coli* [17, 18], which provided important insights for the current work. Human and mouse M2 subunit shares an excellent sequence similarity of $\sim$80 %, whereas for *E. coli* the identity is only $\sim$20 %. A detail of the mouse tyrosyl radical environment has been reported [15, 16]. The crystal structure of human hRRM2 is available in protein data bank, but yet to be published as a journal paper. Therefore, we didn't have the much needed insights, generally discussed by the crystallographers in publications. For these information we relied on the reported holo structures of hP53M2 [14] and mouse. We can summarize the following facts, about the RR active site: The tyrosyl radical is deeply buried in the interior of the protein forming a hydrophobic channel, reaching about 10 Å from the surface. This channel, which is the entrance to the radical site, is about 15 Å wide. It is lined by mainly hydrophobic amino acids like; GLU233 (232), SER238 (237), ASN260 (ASN259), and TYR324 (323) with their side-chain oxygen atoms turned away from the channel. The channel reaches all the way to SER267 (263), PHE241 (240), and SER264 (263) the residues lining the binding site. These residue numbers corresponds to the mouse pdb structure, corresponding human pdb residue numbers are given in bracket. This structural information helped us in identifying the probable entry point/approach of the inhibitors. It also gave us a starting structure to work upon.

We have chosen those ligands with –C(=X)NHOH, where X=O, or NH functionality, as in amidoximes and hydroxamates. They are primarily classified as radical scavengers [1], but most of them also posses additional iron chelating properties [19, 20]. Therefore, we cannot consider these classes of molecules, as exclusively radical scavenger. However, inhibition through radical quenching, and through metal chelation are two different mechanisms [14]. Their approach to respective active site is different, they interact with different pockets of RRM2, and susceptibility towards RRM2 from various species is also different. Therefore, both mode of inhibition needs to be studied separately. In the current work we have studied mode of inhibition of radical scavengers only, but not for metal ion chelators. In order to develop a structure based ligand bound model, we performed a molecular dynamics (MD) simulation study with three radical scavengers (SB-HSC21, ABNM13, and trimidox). We have used four ligands SB-HSC21 (hydroxamic acid), ABNM13 (hydroxyguanidine), trimidox (amidoxime), and compound 7 (thiosemicarbazone) for the current study. SB-HSC21 [21] was reported by Ren et al. in 2002. It is chemically an aromatic Schiff's base of hydroxysemicarbazide. The authors have reported its synthesis, and inhibitory activity against L1210 cell line. Later in 2005 Shao et al. [22] performed the subunit-selective RRM2 assay, and found it to be a potent inhibitor of hRRM2. Trimidox was patented (US5366996) by Howard et al. [23] in 1994. Later in 2000 Szekeres et al. [20] proved it to be an inhibitor of hRRM2. ABNM13 was developed by our group [24, 25] by ligand based pharmacophore modeling, and virtual screening techniques. It was found a promising candidate in HL60 cell line assay. Afterwards, it was found to be a potent inhibitor of hRRM2. All these three molecules were reported to inhibit hRRM2. The difference in biological activity of these compounds may not be significant, but we do not have much choice when it comes to hRRM2 inhibitors. We need to compare our MD results with at least one non inhibitor. We have chosen this compound 7 from one of our earlier reported [26] set of thiosemicarbazones, it has been found inactive in hRRM2 assay.

During the catalytic activity, an electron transfer occurs through the water bridge between the diferric site and the TYR176 phenolic hydroxyl group. This electron transfer is responsible for generating the tyrosyl radical. Therefore, any mechanism that ceases this process can act as a potential inhibitor of RRM2. Throughout the MD simulation process we searched for any interaction between TYR176-OH group and the ligands. Any stable interaction between these groups will definitely disturb the normal electron transfer process, which can result in inhibition of the enzyme. This hypothesis seems reasonable in absence of any reports about how the radical scavengers inhibit the enzyme RR.

In the current work we used QM/MM for geometry optimization of the hRRM2 subunit. A combination molecular docking/dynamics were then used to study the binding modes of the inhibitors. The binding energy was estimated using the eMBrAcE minimization protocol. To establish the stability of the protein under MD simulation condition, holo enzyme was used. *E. coli* and mouse

enzyme were used for comparison. Finally an inactive compound was used as negative control.

Materials and methods

Protein preparation

Human hRRM2 (pdb entry 2uw2) was used for the current study. The structure in the protein data bank exhibited a single iron atom. Human RR however, consists of a di-iron center that was manually built by using the co-ordinates from crystal structure of mouse (pdb entry 1w68). The water bridge between TYR176, and the di-iron center was also not available with the human pdb structures. It was also manually constructed using the co-ordinates from crystal structure of mouse M2 structure (pdb entry 1w68, HOH2035). After manually setting the co-ordinates of di-iron center and the water bridge, we used the protein preparation wizard (Maestro, version 8.5, Schrödinger, LLC, New York, NY, USA, 2008) to refine the protein structure. There were no missing residues, or missing side chains in 2uw2 structure. Only those water molecules within 10 Å of the iron center were used, rest was deleted. Formal charge of +2 was assigned, for both the iron atoms. The ionizable residues were set to their normal ionization states at pH 7, and a restrained energy minimization (relatively higher convergence threshold of a gradient to <0.3 kJ/Å mol) was performed using OPLS-2005 force field. For optimizing the di-iron center we employed a QM/MM hybrid computational method. All QM/MM calculation was performed through QSite module of Schrodinger Suite 2011. Density functional theory (DFT) with the B3LYP functional was used to describe the di-iron center. We used a larger basis set LACVP** on metals and 6–31G** on all other atoms for geometry optimization. The QM region consists of the following regions: (a)The side chains of GLU169, GLU232, GLU266, ASP138, HIS269, HIS172, and one water molecule which coordinate the two iron atoms. (b) The side chain of TYR 176, and another water molecule that forms the electron transfer bridge with the di-iron center. All together 66 atoms were used in the QM region. We have used a high spin ferrous state with total spin $s = 4$, multiplicity $2s + 1 = 9$. The rest of the system was treated as MM region, and all the calculation was performed using OPLS-2005 force field. For molecular docking studies, two of the water molecules which guard the active site entry (Fig. 1a, b) were deleted. This deletion relaxes the residues GLU232 and SER263, which were anchored together by these two water molecules. After deletion of these water molecules the structure was again refined using the protein preparation wizard. The residues were set to ionize at pH 7, followed by a restrained energy minimization using OPLS-2005 force field. This deletion of water Bridge relaxes the protein structure and opens up the active site. The resulting structure is working structure for initial molecular docking simulations. Similar QM/MM calculation was also performed on the mouse pdb structure (1w68). We also performed molecular docking and dynamics calculation on *E. coli* and mouse RRR2 enzyme. We used the pdb entries 1rib and 1w68 respectively for *E. coli* and mouse.

Choice of ligand and their preparation

For the current study we need to choose only those ligands that were experimentally proven to be inhibitors of hRRM2. Moreover, the chosen ligands must be as structurally as diverse as possible. On the other hand, while choosing the ligands we didn't find enough compounds, which are reported as hRRM2 inhibitors. For the current work we have chosen trimidox [1], SB-HSC21 [21, 22], ABNM13 [25], and compound 7 [26] (Fig. 1c). Trimidox ($IC_{50} = 5$ μM, hRRM2) is structurally an amidoxime, SB-HSC21 ($IC_{50} = 11$ μM, hRRM2) is a hydroxy semicarbazone, and ABNM13 ($IC_{50} = 11$ μM, HL60) is a hydroxy guanidine. The order of activity is trimidox > SB-HSC21 ≥ ABNM13. Though they are structurally diverse but all share a common pharmacophore i.e. the hydroxylamino (–NHOH) portion. We have also chosen an inactive compound 7 ($IC_{50} > 500$ μM), which will act as our negative control. After choosing the right ligands they were carefully processed. The structure of the ligands was built in Maestro molecular modeling environment 2008. After drawing the structures they were energy minimized using Macromodel minimization panel using the OPLS-2005 force field and GB/SA water model with a constant dielectric of 1.0. Polak-Ribiere first derivative, conjugate gradient minimization was employed with maximum iterations of 1,000 and convergence threshold of a gradient to <0.05 kJ/Å mol. LigPrep2.0 module of Schrodinger was used to generate possible ionization states at target pH 7.0 ± 2.0. All possible tautomeric states at this pH were also generated using the tautomerizer module of LigPrep2.0. The resulting structures were saved in *.mae format for further experiments.

Molecular docking

All the conformers from the confgen-ligprep output were docked in the RR active site. The purpose has been to provide an initial working structure of the protein–ligand complex, which was later used for further molecular dynamics study. A grid of center of 20 Å × 20 Å × 20 Å on residues ARG330, PHE240, PHE236, SER263, and TYR176 was constructed. A Van der Walls scaling factor

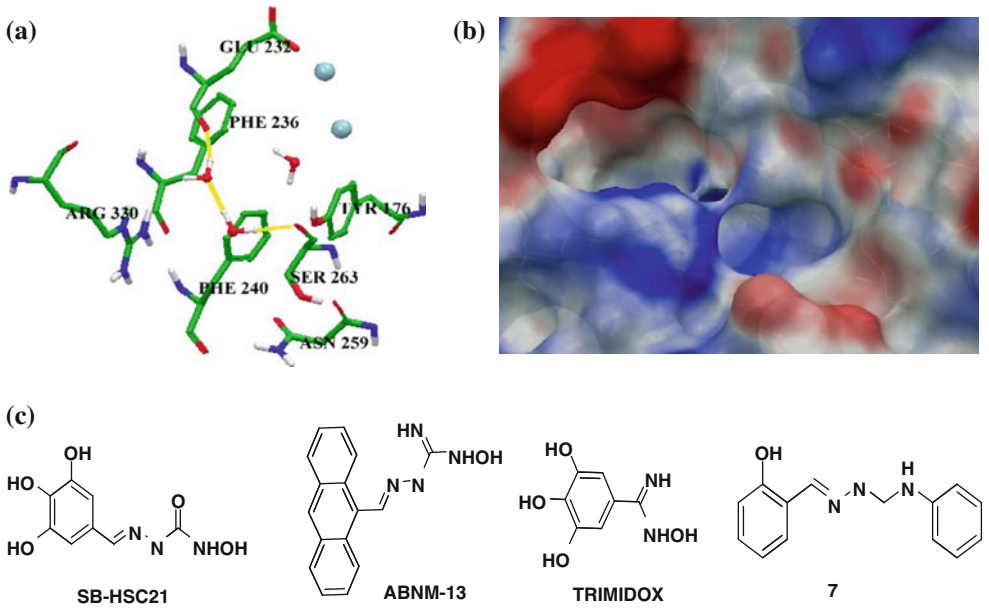

Fig. 1 **a** Bridging by the two water molecules (ball and stick), in between residues GLU232 and SER263. **b** Surface view to explain how this bridging guards the active site pocket. **c** Structures of the ligands chosen for the current study

of 0.80 and partial charge cutoff of 0.15 was used for receptor grid generation. Glide standard precision mode was used for the current docking study. 5,000 poses were used for passing through initial glide screening. Scoring window for keeping initial poses was kept at 100 poses. Best 400 poses were chosen for energy minimization during docking, a distance dependent dielectric constant of 2.0 and maximum number of minimization step of 100 was used. All the docked poses were then clustered based on heavy atom RMSD clustering, with a maximum cutoff of 2.0 Å. Representative docked poses with the best Glide-SP score from each cluster were merged with the protein structure, the complex was used for further MD simulation study.

Molecular dynamics simulation and binding energy analysis

All MD calculations were performed by the Macromodel module of Schrodinger. The initial coordinates for the MD calculations were taken from the docking experiments. The obtained complexes of the three inhibitors (Trimidox [1], SB-HSC2129 [21, 22], and ABNM13 [25]) were used for performing MD simulations. OPLS-2005 force field was employed for MD calculations in continuum solvent with the GB/SA water model within the Macromodel package. A constant dielectric of 1.0 was kept, a cutoff for Van der walls, electrostatic and H-bond interactions were kept at 8.0, 20 and 4 Å respectively. Polak-Ribiere first derivative, conjugate gradient minimization scheme was employed with maximum iterations of 1,000 and a relatively higher convergence threshold of a gradient to 0.125 kJ/Å mol was kept. Before the actual MD simulations were performed, the systems were minimized and pre-equilibrated using a relaxation protocol of 100 ps. A 5 ns MD simulation was performed on each complex and the holo enzyme. During MD simulations, the equations of motion were integrated with a 2 fs time step. The SHAKE algorithm was applied to all hydrogen atoms. The temperature was maintained at 300 K. Trajectories were monitored every 10 ps during the MD runs. Visualization of protein–ligand complexes and MD trajectory analysis were carried out with the Maestro 2011 package.

To calculate the binding energy of association of the ligands with the receptor we used the automated mechanism of Multi-Ligand Bimolecular Association with Energetics (eMBrAcE). eMBrAcE is a part of Macromodel package, through which complexes can be studied using molecular mechanics minimizations and conformational searches. An eMBrAcE minimization is a type of multiple minimization in which each of the specified pre-positioned ligands is minimized, in turn, with the receptor. eMBrAcE calculations were performed on MD sampled structures every 500 ps. The free energies were calculated using OPLS-2005 force field in continuum solvent with the GB/SA water model employing a constant dielectric of 1.0 with 1,000 iterations and a convergence threshold of a gradient to 0.125 kJ/Å mol. eMBrAcE uses two modes for binding energy calculation the interaction mode and the energy difference mode. The Interaction mode uses mutually exclusive atom sets (from receptor and ligand) and calculates interaction energies within and among all such sets.

Only interaction energies between such predefined sets are saved as project properties within the output structure file. Whereas, the energy difference mode applies the energy calculation to the receptor, then for each ligand in turn. Finally it reports the energy difference. For the current work we employed energy difference mode.

The binding energy is calculated as

$$\Delta E = E_{\text{complex}} - E_{\text{ligand}} - E_{\text{protein}}$$

The full effects of relaxation (100 ps pre-equilibration) and solvation (continuum solvent with the GB/SA water parameters) are included in this calculation.

Results and discussions

In the enzyme RR, the M2 subunit is responsible for generating the free radical that reduces ribonucleotides to their corresponding deoxyribonucleotides. This reduction occurs via a single electron transfer from TYR176. The free radical on TYR176 is initiated by the radical-generating, diiron (III/IV) state via a single electron transfer, through a water molecule forming a bridge between the hydroxyl oxygen atom of TYR176, and the iron center [3, 27, 28]. The non-haeme di-iron center of hRRM2 is unique; Torrent et al. [23] have described in details the mechanism of activation of the di-iron center to generate the free radical. They have proposed an activation cycle which follows like: The active state $Fe^{II}{\cdot}Fe^{II}$—formation of the μ-oxo bridge, by addition of oxygen $Fe^{III}{\cdot}{O_2}^{2-}{\cdot}Fe^{III}$ (Compound P)—mixed valence state $Fe^{IV}{\cdot}{O_2}^{3-}{\cdot}Fe^{III}$ (Compound X)—resting state $Fe^{III}{\cdot}Fe^{III}$ via formation of the Tyrosil radical (TYR-O$^{\cdot}$). Yun et al. [13] later proved that addition of oxygen to the $Fe^{II}{\cdot}Fe^{II}$ active state for the formation of Compound P is the rate determining step in the entire process. Once this free radical is generated, it is very quickly transferred by the relay mechanism to the catalytic active site in M1 subunit. It would be impossible to arrest the normal activity of the enzyme once this radical is generated. Hence, we hypothesize; (1) The inhibition process must have initiated before the formation of Compound P. Therefore, the $Fe^{II}{\cdot}Fe^{II}$ state of iron should be ideal during the docking/MD simulation studies. (2) The inhibitors may act by disrupting the water bridge between TYR176 oxygen and iron thereby the electron transfer is ceased and the free radical is not generated. Throughout the simulation process, we have monitored this disruption, and searched for any interaction between the inhibitors and TYR176 oxygen.

In the 1st phase of our study, we have thoroughly studied the active site of RR. The entry to the active site is guarded efficiently by residue ARG330, and by a water bridge between residues SER263 and GLU232. These two water molecules (Fig. 1a, b) shield the 10 Å hydrophobic tunnel. Inhibitors binding to the RR active site should replace these water molecules to get access to the hydrophobic tunnel, lying underneath. We generated the initial protein–ligand complexes by docking the ligands with the holo protein structure. To generate this initial poses, we need to relax the entry point to the active site. If this relaxation protocol is not performed before docking, we may end up with poses, which are away from the entry point, or poses that show false interactions. Therefore, in order to gain access to the active site, and to get a reasonable/relaxed initial structure we have manually deleted the two water molecules. We have used Glide SP, docking to generate the initial working structures. The poses for each molecule were clustered after docking with a RMSD cutoff of 2.0 Å. Each representative pose from every cluster was chosen for building the protein–ligand complex. From SB-HSC21 and ABNM13 we obtained a single cluster, for trimidox we obtained two distinct clusters (for *E. coli* enzymes we obtained only one cluster). Glide scores for this initial docking poses are not presented. At this stage our primary aim has been to generate a plausible initial working structure for our MD study. After obtaining these initial co-ordinates, the protein–ligand complexes were used for further MD study.

We observed a number of H-bonds during the MD simulation process. Some of them were observed in all, some occurred in majority, and some in very few of the sampled structures. We are discussing the H-bonding interactions that were observed in either all, or in majority of the samples. We are not discussing those that occurred in very few of the sampled trajectories.

The working structures of iron center and the ligands

One of the most important outcomes from QM/MM study is the structure of the diiron/radical center. The active center has been generated under oxidizable conditions. The initial coordinates for the diiron and the μ-oxo bridge were obtained from mouse pdb structure (1w68). After a QM/MM optimization run, we observed the di-iron active center for human enzyme in very close match with the earlier reported mouse enzyme structure. Computational [28] and spectral studies [29, 30] for the di-iron center of RRM2 described it as ferromagnetically coupled high-spin species. In accordance to these studies we have chosen a total spin $s = 4$, resulting in multiplicity of $2s + 1 = 9$, for the spin system. The hRRM2 iron site is buried in a four-helix bundle, which is coordinated by the two histidines and the three glutamic acid carboxylate side chains. The Fe1, close to the TYR176, coordinates with ASP138 and HIS172. During minimization, in few of the trajectories we observed a bi-dented coordination of ASP138 carboxyl group with Fe1. However, a single coordination

was observed in the lowest energy conformation. The other iron atom, Fe2 is coordinated by GLU232, GLU266, and HIS269. Residue GLU169, coordinates with both the iron Fe1 and Fe2, and behaves as bidentate ligand. The optimal Fe1–Fe2 distance was found to be 3.68 Å, as compared to mouse 3.32 Å and *E. coli* it was 3.3 Å. The dihedral angle between Fe1–O–Fe2 was found to be 133 degrees. Hydrogen bonding was observed between TYR176 and a single water molecule, hypothesized to bridge between the diiron and the radical center. The distance between the Fe1 and water molecule was found to be 4.57 Å, much longer than mouse 3.84 Å. The structure of di-iron of mRRM2 was found to be very similar to hRRM2. Though there are slight differences observed in co-ordination patterns and distances (Fig. 2a, b).

We also need to use the correct tautomeric forms for the ligands during docking and MD studies. Amidoximes and hydroxyguanidines may be present in two tautomeric forms; the amino oxime state, and imino hydroxylamine state [31]. For SB-HSC21 hydroxamic acid tautomer will be favorable, and for compound 7 the thiocarbamyl hydroxamate must be favorable. However, we have not relied entirely on the previous reports on tautomerization for similar molecules. Instead we have generated all the possible tautomeric forms, which were then screened through tautomerizer, at target pH of 7.0 ± 2.0, and a tautomer probably cutoff threshold of 0.01. The tautomerizer program will assign a probability to each tautomeric form. Tautomers for the given input structure are produced in order of probability. We subjected all the survived tautomer for docking, the top survived tautomer(s) is considered as the most probable tautomeric state under the applied conditions, and were used for further studies.

We have also performed a QM-MM calculation of 1w68 (mouse pdb RRM2). We observed that the di-iron center was extremely stable under the minimization conditions. The co-ordination pattern also remained similar to that observed in the experimental structure. Modest deviations were observed in the water bridge between the TYR177 and the di-iron center. The distance between water molecule and the di-iron center was observed to be 3.03 Å, but in the crystal structure this distance was around 3.87 Å. Therefore, during the minimization the water bridge has been strengthened, and returned a structure with optimal distance for electron transfer. This calculation served an additional validation protocol that confirms the adopted methodology returns a structure consistent with the reported experimental structure.

Geometry of the holo enzyme

A 5 ns MD simulation study of the holo enzyme structure of human RRM2 was performed. The working structure generated from the QM/MM calculation was used. The aim of this MD study is to check the stability of the working holo structure during the dynamics run, and to also compare the MD results obtained from other ligands. We monitored the disruption of the water bridge, the Fe–Fe distances, and the RMSF values of important amino acid residues (Fig. 3).

Throughout the MD-simulation run we observed the water bridge between residues TYR176, and the di-iron center has not been disturbed. Further, analysis of the Fe–Fe distances revealed the deviation never goes beyond 1 Å. The RMSF values for none of the intrinsic amino acid side chain goes beyond 2 Å. All these observations suggest the generated working structure of the holo protein is stable under the applied MD condition. The working structure can therefore be used for further simulation studies.

Interaction of SB-HSC21 with RR

SB-HSC21 was reported by Ren et al. [21] structurally it is a tri-phenolic Schiff's base of hydroxysemicarbazide. Later it was found to be an inhibitor of hRRM2 [22]. During MD simulation we have identified PHE240 makes a dramatic conformation shift (Fig. 4a–c) to allow the entry of SB-HSC21. Figure 4b shows the surface alignment of pre and post MD simulation studies. It clearly reveals how PHE240 guards the active site (grey surface), and later opens up during MD simulation (blue surface). In order to study its dynamic behavior, we plotted the inter residue distances of PHE240 at various intervals (Fig. 4c). This dramatic conformational shift of PHE240 started after 500 ps (>3 Å), after a brief halt for 500 ps more, it started steeply rising till 1,200 ps. Afterwards, remained relatively stable throughout the MD simulation of 5 ns. From this study we found, PHE240 protects the radical site from the outside environment. When the ligand approaches the narrowed channel, it induces a number of residues, especially PHE240 to move significantly. This movement, allowed the approaching ligand to fit in correct orientation to the active site. We also analyzed the movement of other active site residues viz., PHE236, ARG330, GLU232, ASN259 and SER263. These residues didn't shift as much as PHE240, but moved enough so as to accommodate the approaching ligand.

All the three hydroxyl groups on the phenyl ring of SB-HSC21 were involved H-bonding with residues GLU232 and/or ARG330. The 2nd position hydroxyl formed a stable hydrogen bonding (average distance 2.34 Å) with the peptidyl carbonyl of GLU232, which was observed in all the sampled trajectories. 3rd and 4th hydroxyl group formed hydrogen bonds with the guanidine sidechain of ARG330. These described H-bonds were observed in majority of the sampled trajectories. The average H-bond

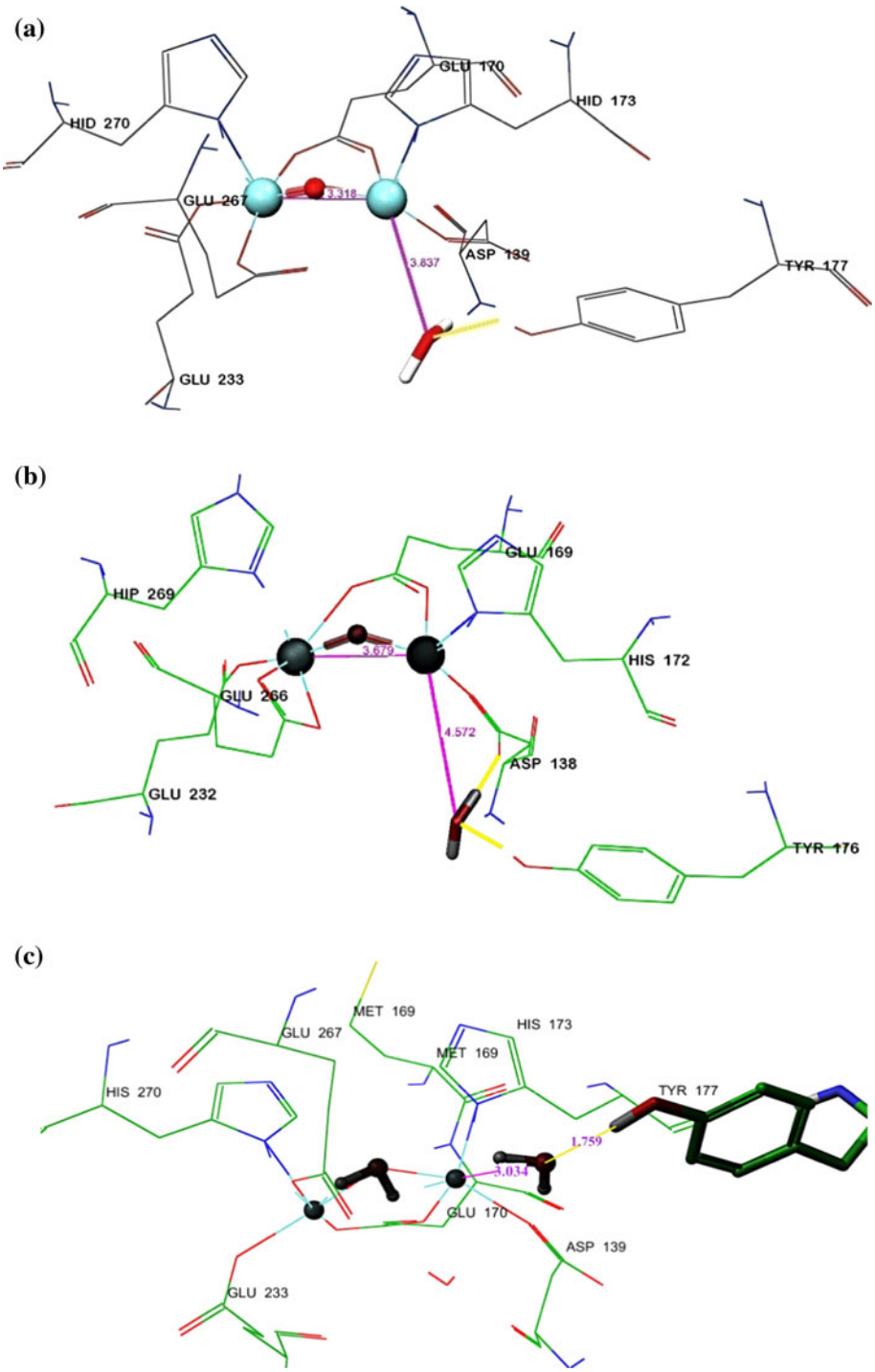

Fig. 2 Structure of the di-iron center **a** Mouse pdb structure 1w68. **b** Structure of human (hRRM2) di-iron center obtained after QM/MM optimization study. **c** Structure of mouse pdb structure after QM-MM optimization

distances of 3rd and 4th hydroxyl group with ARG330 was found to be 2.89 Å and 3.31 Å respectively. These observations may explain why some poly phenolics compounds were earlier reported as inhibitors of M2 subunit of RR. Another stable H-bond was observed between the carbonyl oxygen of hydroxamic acid, and ASN259 with average bond length of 2.41 Å. It remained throughout the MD run, and occurred in all the sampled trajectories. For the entire MD simulation run we also observed another stable H-bond between the hydroxyl amino part (–NHOH) of the inhibitors with TYR176 oxygen replacing one of the water molecule. This water forms the bridge between TYR176 and the diiron (II/II)-O2 adduct and brings about the electron transfer. This H-bond was observed in all the sampled trajectories, and forms immediately with the initial stabilization period of 100 ps. It remained stable during

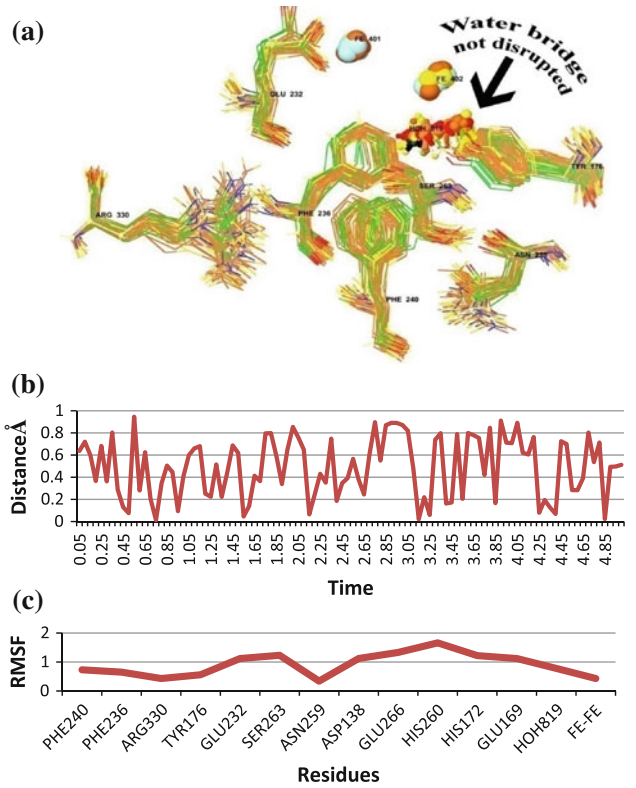

Fig. 3 **a** Trajectory analysis of the holo enzyme. **b** Fe–Fe distances. **c** B-factor for a few important amino acid residues during the MD-simulation

long MD runs with average bond length of 1.84 Å. Probably, this disruption of the water bridge ceases the electron transfer process, which inhibits the propagation of the radical generated by the iron complex to TYR176.

We also performed MD simulation with holo enzyme under similar conditions, which revealed: (a) the amino acid residues PHE240, PHE236, SER263, and ARG330 did not shift significantly, as compared to the MD simulation of SB-HSC21 with hRRM2, (b) the water bridge between the di-iron center and TYR176 has not been disrupted. Therefore, the observed conformational shifts in the amino acid residues, and the disruption are induced by the inhibitor.

Interaction of ABNM13 with RR

ABNM13 is a potent inhibitor of RR, developed from our lab [24, 25]. Chemically it is a *N*-amino-*N*′-hydroxy guanidine Schiff's base of anthracene-9-carboxaldehyde. It's interaction with RR was studied by 5 ns MD simulation. Initial co-ordinates for MD simulation study of ABNM13 were obtained by docking ABNM13 with RR working structure. After obtaining these initial co-ordinates, the system were pre-equilibrated using a relaxation protocol of 100 ps. 500 posses were sampled at regular interval for trajectory analysis. After the MD simulation, following are the important observations: Fig. 5a–c: (a) Regarding ARG330: The guanidine part of ARG330 deviated to almost 4 Å to accommodate the larger anthracene ring in the active site. We observed, ARG330 undergoes a continuous conformational shift till 2.5 ns with maximum deviation of 4.97 Å. Towards the latter half of the simulation, from 2.5 to 5 ns it remained stable, without significant dynamic shift in conformation. (b) Regarding PHE240 and PHE236: Similar adjustments were also found in other residues like PHE236 and PHE240. For PHE240 we observed a conformational shift, but not as dramatic as that of SB-HSC21. We observed significant shift from 250 to 1,500 ps, followed by a steep decrease around 1,500 ps. The deviation continues to decrease in the same fashion till sometime, but remained stable afterwards. One of the possible reasons may be the favorable hydrophobic interactions that we observed between the anthracene ring of ABNM13, and the phenyl ring of PHE240 and PHE236 (Fig. 5b). These interactions must have pulled residues PHE240 and PHE236 closer to the anthracene ring and as a consequence reduces the inter-residue distances. We observed favorable π–π interactions between the anthracene ring of ABNM13 and the phenyl side chain of PHE240 and PHE236, in majority of the sampled poses as shown in Fig. 5b. (c) Regarding the H-bond with TYR176: We observed strong H-bonding interaction between the hydroxyl amino part (–NHOH) of ABNM13 and TYR176 oxygen by replacing one of the water molecule, similar to that observed in SB-HSC21. This hydrogen bond was observed in all the sampled trajectories and forms immediately with the initial stabilization period. It remained stable with average bond length of 1.79 Å. When we compared with the holo enzyme, the conformation remained extremely stable throughout the MD simulation. The deviations observed in holo enzyme, and ABNM13-protein complex during MD simulation is significant, and induced by the ligand.

Interaction of trimidox with the RR active site

Trimidox is chemically a poly phenolic amidoxime. It is reported to be a potent and selective inhibitor of hRRM2. Being a very small molecule, trimidox experiences significant freedom when docked in the active site of the enzyme. Therefore, we can cluster the initial docked poses into two distinct categories: cluster 1, those docked poses where the –NHOH is toward TYR176 and, cluster 2, where the phenolic hydroxyl groups are towards TYR176.

For cluster-1 (Fig. 6a), we observed a similar H-bonding between the amidoxime –NHOH and phenolic hydroxyl of TYR176, with average H-bonding distance of 1.98 Å. We also observed that the imino =NH group participate in

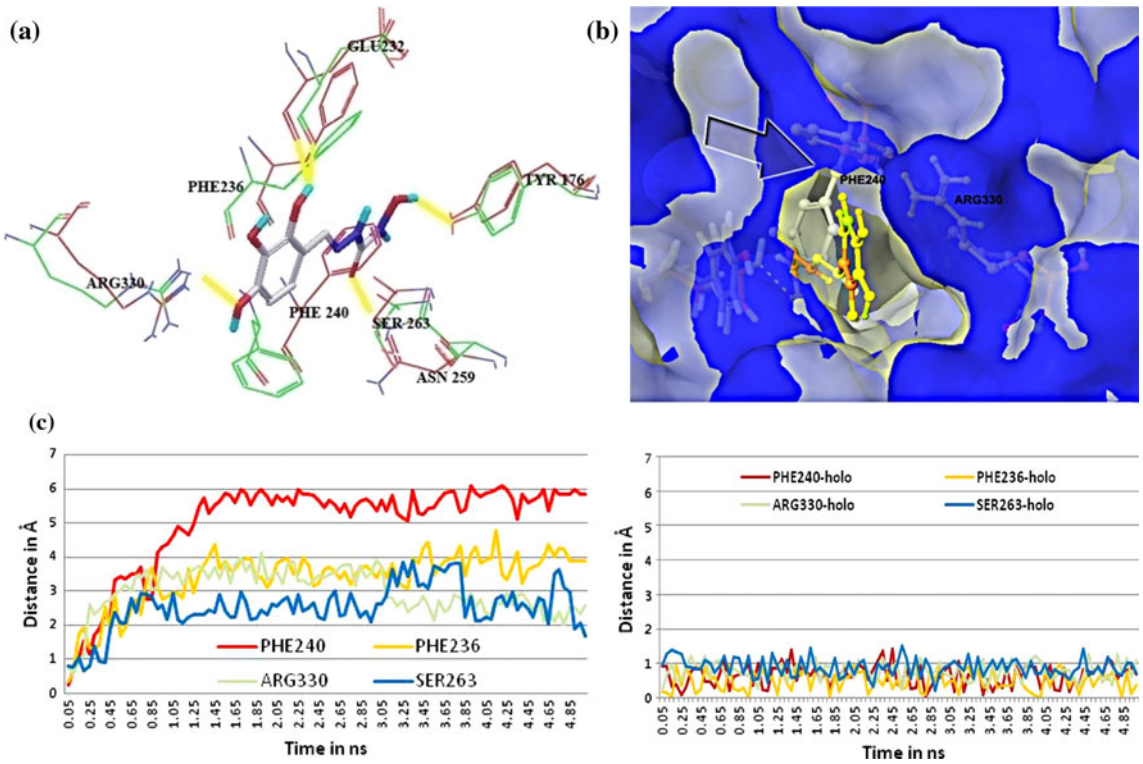

Fig. 4 **a** Poses of SB-HSC21 before (*red* carbon) and after (*green* carbon) MD simulation. **b** Aligned surface views before (*grey*) and after (*blue*) MD simulation. **c** Deviation from the initial position of different amino acids during the entire MD simulation run, 1st for simulation with SB-SHC21, and second without any inhibitor

H-bonding interaction with ASN259, amide (–C=O) carbonyl group in most of the sampled trajectories with an average distance of 2.14 Å. In some of the sampled trajectories the phenolic –OH groups participated in H-bonding with either ARG330 or with ASN259. We also observed two residues PHE240, PHE236 and SER263 making a significant conformational shift to give way to the incoming ligand.

For cluster-2 (Fig. 6b) we observed stable H-bonding between the phenolic hydroxyl groups of trimidox and phenolic hydroxyl of TYR176. In majority of the sampled trajectories, this H-bonding was observed with the 4th hydroxyl group with average distance of 1.84 Å. In very few sampled structures we found the 3rd hydroxyl making this H-bond with TYR176. In some trajectories we found this 3rd hydroxyl group participating in an H-bonding interaction with ASN259. For this MD cluster, we found a significant movement for residues PHE236, PHE240, and SER263. The movement of these residues widened the end of the active site channel so that the bulkier phenyl group of trimidox could be accommodated.

Post MD simulation poses for cluster-1 and cluster-2 were aligned (Fig. 6c) to study the movements for residue PHE240, PHE236 and SER263. We observed no significant difference in between clusters 1 and 2. The plots also reveal similar facts (Fig. 6d); the deviation was raised to ~4.0 Å till 1 ns and remained stable afterwards.

When we compared our dynamics results with the holo hRRM2 enzyme, the deviations of the aminoacids has been found significant. The observed shifts in the amino acid residues, and the disruption of the water bridge are induced by the inhibitor.

General observations for all the three ligands

All the three ligands are structurally different, but they share a common hydroxyl amino (–NHOH) pharmacophore. All of them form the H-bond with TYR176 hydroxyl group, replacing the water molecule that forms the water bridge. For all the three ligands, this H-bond was formed during the initial stabilization period of 100 ps, and was observed in all the sampled trajectories with average bond length <2.00 Å. We believe this observed strong H-bonding interactions is the key to RR inhibition by radical scavengers. The formation of this H-bond must have altered the electron density on the TYR176 phenolic –OH. As a result the water bridge between TRY176, and di-iron center is disrupted. We have not calculated the exact quantum of change in electron density, before and after binding of ligands. However, we have compared the

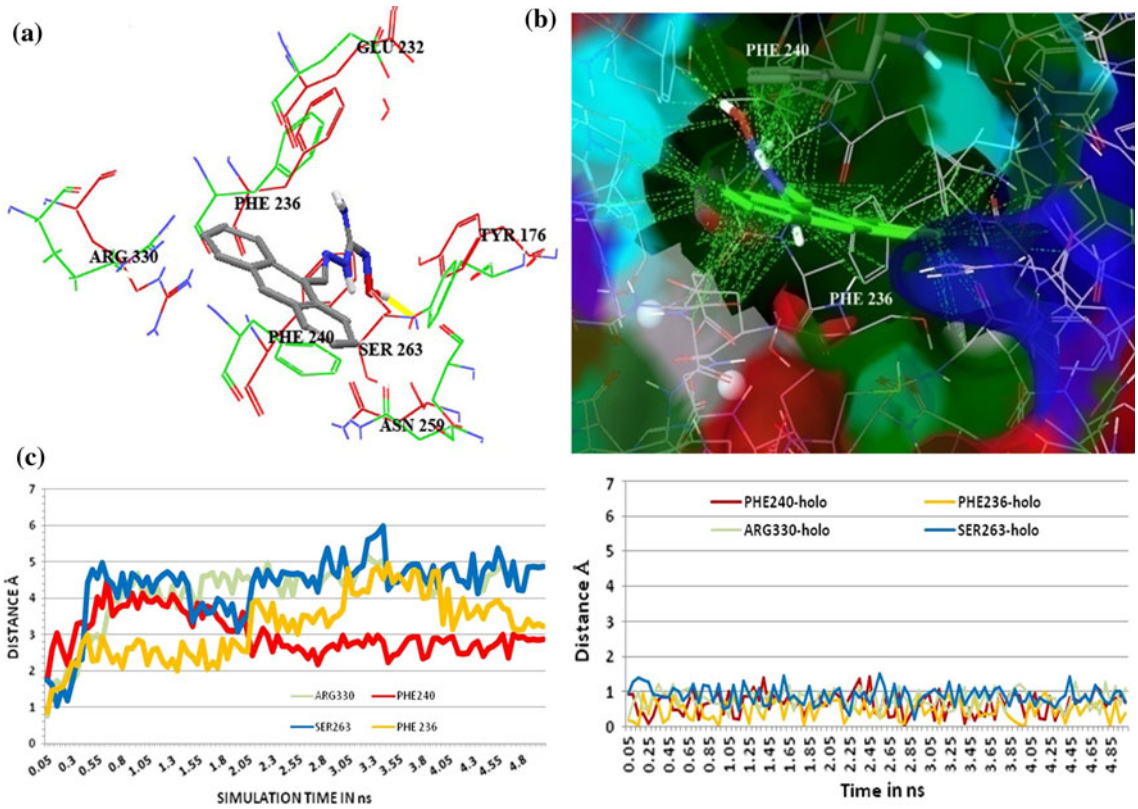

Fig. 5 **a** Aligned Pose of ABNM13 before (*red* carbon) and after (*green* carbon) MD simulation. **b** Surface views showing the *yellow lines* as hydrophobic favorable contacts with the receptor. **c** Distance deviation plots of different aminoacids during the entire MD simulation run

disruptions during binding of different ligands (Fig. 7). We have also compared it with the holo enzyme, and one non-inhibitor. We observed, H-bonding of the ligands with TYR176 phenolic –OH upsets the entire system: TYR176–HOH–di-iron. The water molecule bridging the TYR176 and the di-iron center moved significantly away from their initial co-ordinates and the H-bonding network has completely been disrupted. This disruption must have ceased the radical generation process; as a consequence they inhibit the enzyme.

From the MD simulation study we found, the active site tunnel is extremely malleable, and can accommodate different sizes of ligands (Fig. 8). After a 5 ns dynamics simulation we identified four amino acid residues ARG330, SER263, PHE240 and PHE236 are mainly responsible for guiding the ligands to the underlying channel, which is terminated by TYR176.

A close investigation of the active site tunnel reveals the presence of gatekeeper residues, at two different stages (Fig. 9a–d). The outer gatekeeper ARG330 is present on the surface, and controls the initial entry/recognition of the ligand. After this Gate-1 is opened the ligand faces Gate-2, which is guarded by three amino acid residues SER263, PHE236, and PHE240. On approach of the ligands these three residues open up suitably, so that the incoming ligand can go through. Therefore, we describe that the active site as guarded by two gates (1 and 2); the incoming ligand has to open these two gates to get access to the underlying TYR176 residue. We compared the conformational shifts for residues PHE236, PHE240 and SER263, for all the three different ligands. For SB-HSC21 and ABNM13 we observed lesser movement of PHE236, throughout the simulation process. However, residues PHE240 and SER263 make the required conformational shift for these two ligands that allowed them to go through the gate-2, and make the intrinsic interaction. For both the poses of trimidox we found a significant shift in conformation of PHE236 along with SER263 and PHE240.

We were also interested to know the consequence of a 5 ns MD-simulation on the architecture of the di-iron center; it might not retain its original state. We analyzed the structure of the di-iron center for every sampled trajectory. The di-iron center retained its original geometry, and no significant difference was observed during the entire run. Figure 10, shows the plot of Fe1–Fe2 distance for hRRM2 from the optimum i.e. 3.68 Å. Average deviation that was observed was around $\sim$0.4 Å for all the ligands and the holo enzyme. Probable reason for this minimal deviation may be due to the coordination pattern for both the iron atoms with several amino acid side chains.

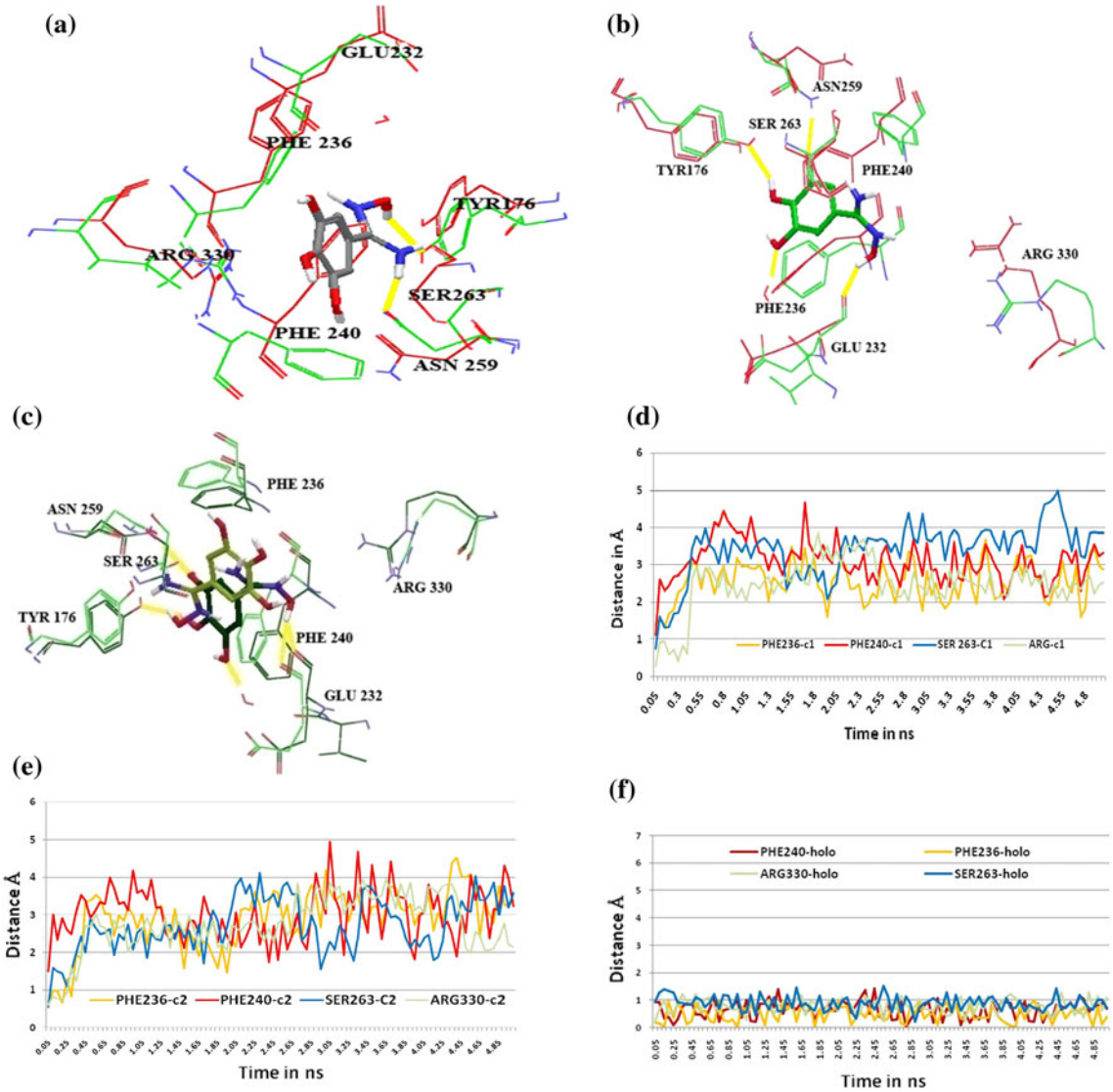

Fig. 6 **a** Aligned pose of trimidox-cluster-1, before (*red* carbon) and after (*green* carbon) MD simulation. **b** Aligned pose of trimidox-cluster-2, before (*red* carbon) and after (*green* carbon) MD simulation. **c** Aligned pose of trimidox-cluster-1 (*dark*) and trimidox-cluster-2 (*light*) MD simulation. **d** Deviation of different aminoacids from their initial position during MD simulation with trimidox-c1. **e** With trimidox-c2. **f** without any inhibitor

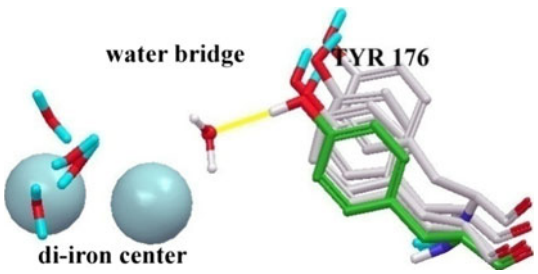

Fig. 7 Water bridge between TYR176 and the di-iron center. The holo hRRM2 structure is shown in *green* carbons corresponding water molecule in ball and stick model. Structures in *light grey* carbons represent the structures after MD simulation with different ligands

This strong coordination retains the position and geometry of the di-iron center throughout the MD-simulation run.

Binding energy calculations

The binding energy for all the three ligands at different intervals was calculated using the eMBrAcE algorithm of Macromodel. The structures were sampled every 500 ps and subjected to eMBrAcE binding energy calculations. After calculating the binding energies at regular intervals of MD simulation we obtained different free energy values. These values reflected the quantum of molecular interactions; i.e. an indirect reflection of the biological activity. The biological activity of selected ligands are as follows,

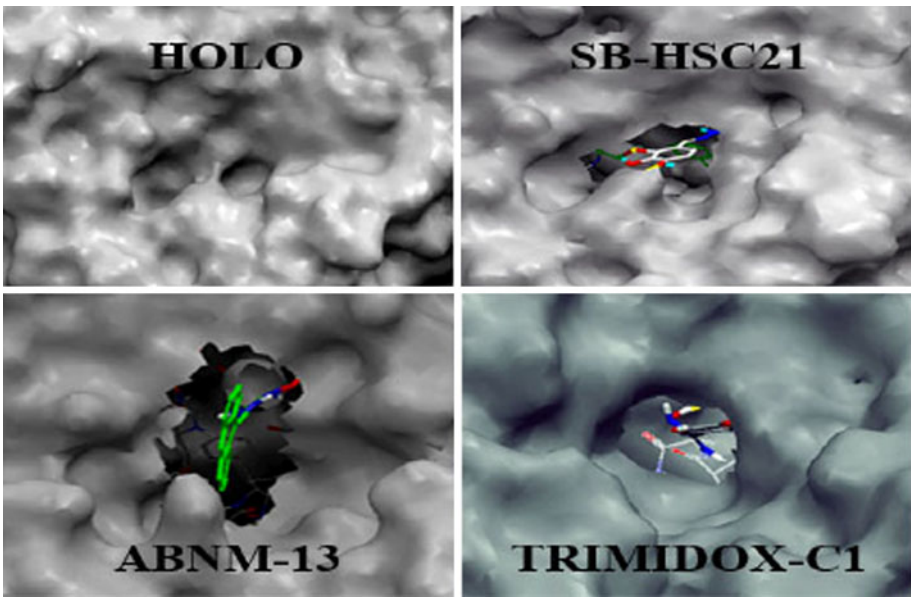

Fig. 8 Surface views of active site of RR with different ligands, depicting the malleability of the active site

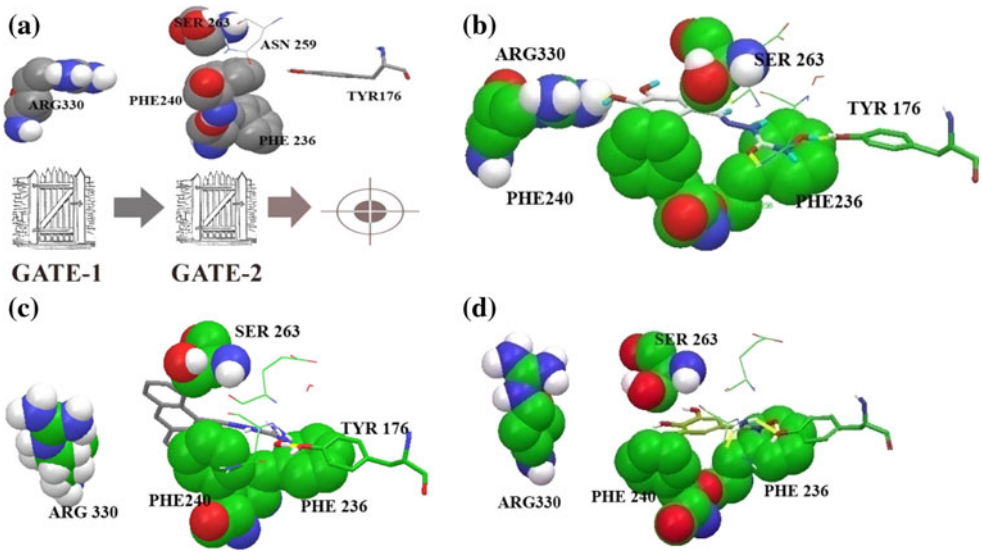

Fig. 9 Residues ARG330, PHE240,PHE236 and SER263 depicted in space filling spheres. Explains the gate keeping mechanism. **a** The holo structure Gate1 keeper ARG330, Gate-2 keeper PHE240, PHE236, and SER263 in Grey carbons. Other figures shows how the gate keeping mechanism works for different type of inhibitors like **b** SB-HSC21 **c** ABNM13 **d** trimidox-C1. Shown in space filling spheres *green* carbons

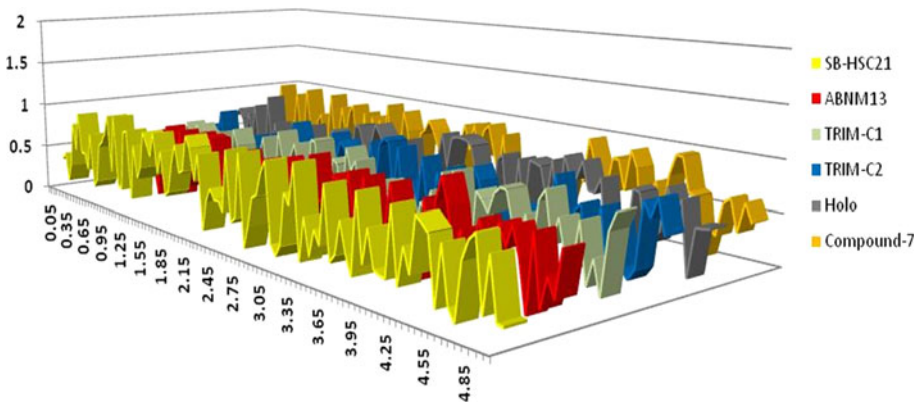

Fig. 10 Fe1-Fe2, distance plots for various ligands used for the study as a function of MD-simulation time

trimidox (IC_{50} = 5 μM, hRRM2), SB-HSC21 (IC_{50} = 11 μM, hRRM2), and ABNM13 (IC_{50} = 11 μM, HL60). The difference in biological activities between these three compounds are not significant, but we can at least assign the order of activity, which is trimidox > SB-HSC21 ≥ ABNM13. After eMBrAcE calculations, following details

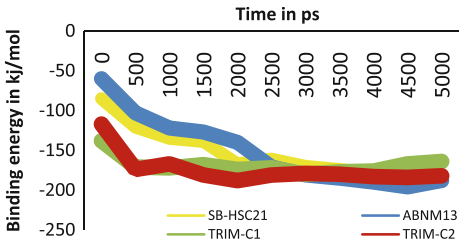

Fig. 11 Binding energy curve for the selected ligands using eMBrAcE. Zero time depicts the resulting binding energy of the ligands with the enzyme after docking and subsequent stabilization/relaxation period of 100 ps, just before the commencement of MD simulations

were observed (Fig. 11): For SB-HSC21, we observed a steep increase in binding free energy till 2 ns, afterwards, it remained steady throughout. On the other hand ABNM13 took a little bit longer time (2.5 ns) to reach the steady state. The resulting binding energy curve for both these compounds revealed a similar pattern. Considering both (SB-HSC21 and ABNM13) as equally potent, this observation is in congruence with their experimental values. For trimidox, the zero time on the X-axis i.e. the starting structure (the docked complex + initial stabilization period for MD simulation) yielded a binding energy value of −138.08 kJ/mol (cluster-C1) and −117.84 (cluster-C2). Compared to SB-HSC21 (−85.12 kJ/mol) and ABNM13 (−60.85 kJ/mol) the binding free energy was significantly low for trimidox than the starting structures of other two ligands. Trimidox, being a small molecule engages itself to various molecular interactions more rapidly that the other two bigger ligands. Therefore, during docking and subsequent stabilization/relaxation period of 100 ps it must have reached the core of the active site, and engaged itself in a few molecular interactions. Thereafter, it reached quickly to a steady state after 500 ps, and remained stable throughout the MD run. Ultimately, it reached a binding free energy values similar to SB-HSC21 and ABNM13. No fluctuations in binding energy value were observed from 500 to 5,000 ps. This steady free energy curve reveals trimidox have not dissociated from the already engaged interactions within the observed 5 ns MD time frame.

Comparison with mouse and *E. coli* enzymes

In order to further validate our results, we performed similar docking and MD simulation studies using *E. coli* and mouse enzymes. One of the most significant differences between the *E. coli* and mammalian M2 proteins is in their sensitivity towards radical scavengers. For example, the concentration of hydroxyurea needed for inactivation of M2 is strongly dependent on species, and the mammalian and viral enzymes seem more susceptible than the *E. coli* M2. Further, the presence of substituent on the hydroxyurea molecule influence the inhibition and, generally, a bulky substituent reduces the effect of inhibition of *E. coli* M2 [32]. The entrance to the hydrophobic channel in mouse and *E. coli* M2 seems to explain the difference in reactivity. Figure 12a, b shows more accessible human/mouse M2 radical site as compared to *E. coli* site. We performed similar MD calculations on *E. coli* enzymes, as it has been performed with human enzymes, as an additional validation protocol. We are presenting a comparison that clearly suggests low affinity of radical scavengers towards *E. coli* protein. A post MD simulation comparative study of human with *E. coli* enzymes reveals the more closed nature of the active site for the later. The presence of much smaller side chain of serine (SER237) in human enzyme instead of tyrosine as for *E. coli* makes the human enzyme radical site more accessible.

MD simulation clearly reveals relative open architecture of the hRRM2 tunnel gate leading to the radical site. Figure 12c, d presents the surface view for both the enzymes. For hRRM2 all the ligands successfully opened the gates (discussed in earlier sections), and accessed the underlying tunnel to the Tyrosine residue (TYR176). For *E. coli* M2, we didn't observe such kind of gate opening mechanism during 5 ns MD-simulation run.

Our observations are consistent with the experimental values, which stated human enzymes are more susceptible towards radical scavengers than *E. coli*. Table 1, presents a comparison of both human and *E. coli* enzymes, clearly revealing the differences.

Comparison with holo enzymes and a non-inhibitor

We compared the root mean square fluctuations (RMSF) of side chains of different residues with the holo enzyme, which acted as a control for the study. We found, residues ARG330, PHE240, and PHE236 moves significantly during MD simulation run, for all the three inhibitor. The water bridge between TRY176 and di-iron is completely disrupted during the MD-simulation run with the three ligand protein complexes. Whereas, this water bridge remained extremely stable during MD-simulation studies with the holo enzyme. Therefore, the disruption that we have observed during MD-simulation study of ligand–protein complexes is due to interaction of the ligand–NHOH group with TYR176 hydroxyl group. The water bridge is stable, and disruption does not occur naturally, but induced by the incoming ligands.

We also compared the RMSF of the residues, which coordinates with the di-iron center. We found, the di-iron center remained stable throughout the run time and for all the performed simulations (holo and protein–ligand complexes) (Fig. 13).

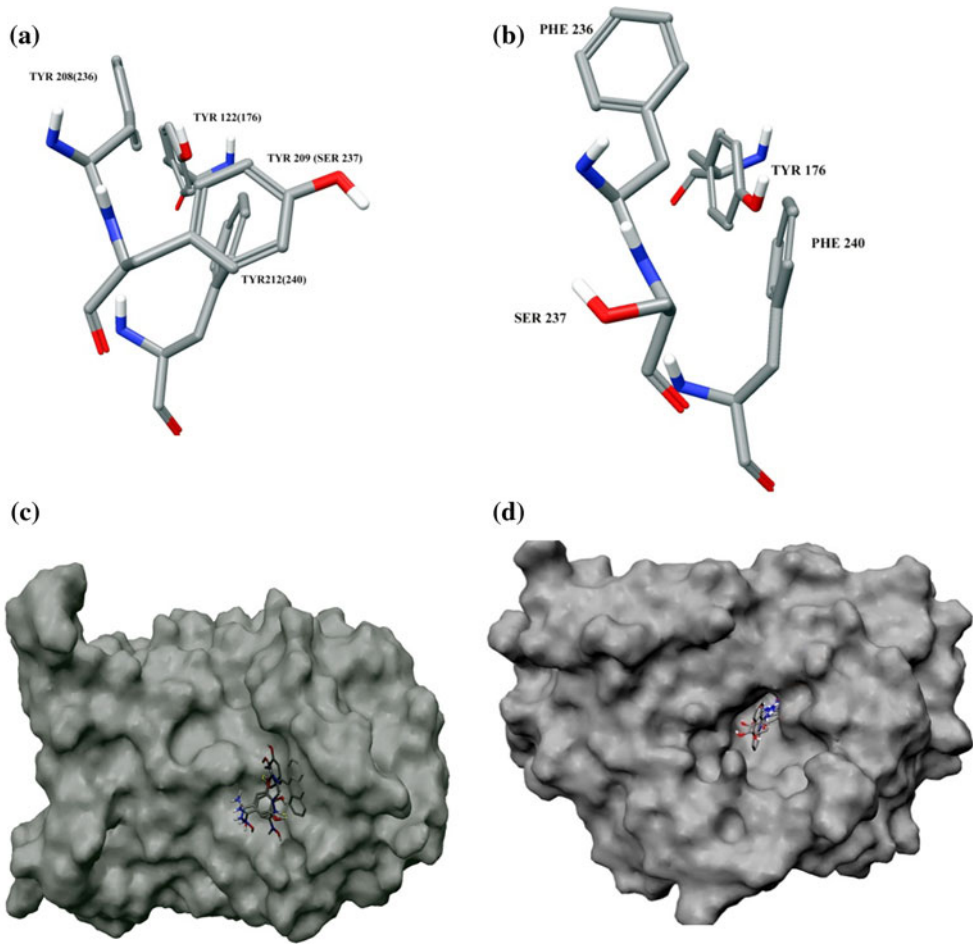

Fig. 12 **a** Entry to the radical site of *E. coli* **b** Much open entry for human (hRRM2) radical site. **c** Post MD simulation poses of all the ligands (trimidox, ABNM13, and SB-HSC21) to the *E. coli* active site. **d** Post MD simulation poses of all the ligands to the hRRM2 active site

Table 1 Comparison of MN-results for human/mouse RRM2 enzymes with that of *E. coli*

Parameters	Human/mouse	*E. coli*
Docking scores[a]	High	Very low
Hydrogen bonding with TYR176	Majority of sampled structures	Never observed
Penetration to the active site gorge	Always	Never observed
Disruption of water bridge	Disrupted	Not disrupted
Susceptibility for radical scavengers	More	Less

[a] Docking was performed with trimidox, ABNM13, and SB-HSC21

To further validate our MD protocol, we need to run the same MD simulation study with experimentally proven non-inhibitors. Earlier we have reported a set of thiosemicarbazones, and tested them against hRRM2. Most of these reported compounds were found inactive, and a few with moderate activity. These molecules forms the ideal non-inhibitors for cross-validating our results. These molecules are aromatic Schiff's bases of thiosemicarbazide, but do not have the intrinsic pharmacophoric feature (–NHOH). This kind of inactive molecules allow us to compare the effect of the –NHOH group in disruption of the water bridge, and ultimately the inhibition of hRRM2. We have chosen a single representative molecule, and followed the same modeling protocol that has been used for the other inhibitors. Initial docking pose for compound 7, was generated by Glide-SP docking. We followed the same procedure, as we have used it for the other ligands.

After getting the docked pose, the docked ligand and the protein was merged, and carried out the MD simulation, which revealed the following: (a) The initial docked pose for compound 7 was entirely different from all the three inhibitors, (b) the water bridge between TYR176 and the di-iron center has not been disrupted during the 5 ns MD simulation, (c) no hydrogen bonding was observed between TYR176, and compound 7, and (d) The residues guarding the active site tunnel (ARG330, SER263, GLU232, PHE240, PHE236, and ASN259) remained relatively stable, and unaltered during the MD process. These observations suggest the tyrosine radical, and the di-iron centers are well protected. The movements/shifts of these residues that we have observed during the MD simulation for the three

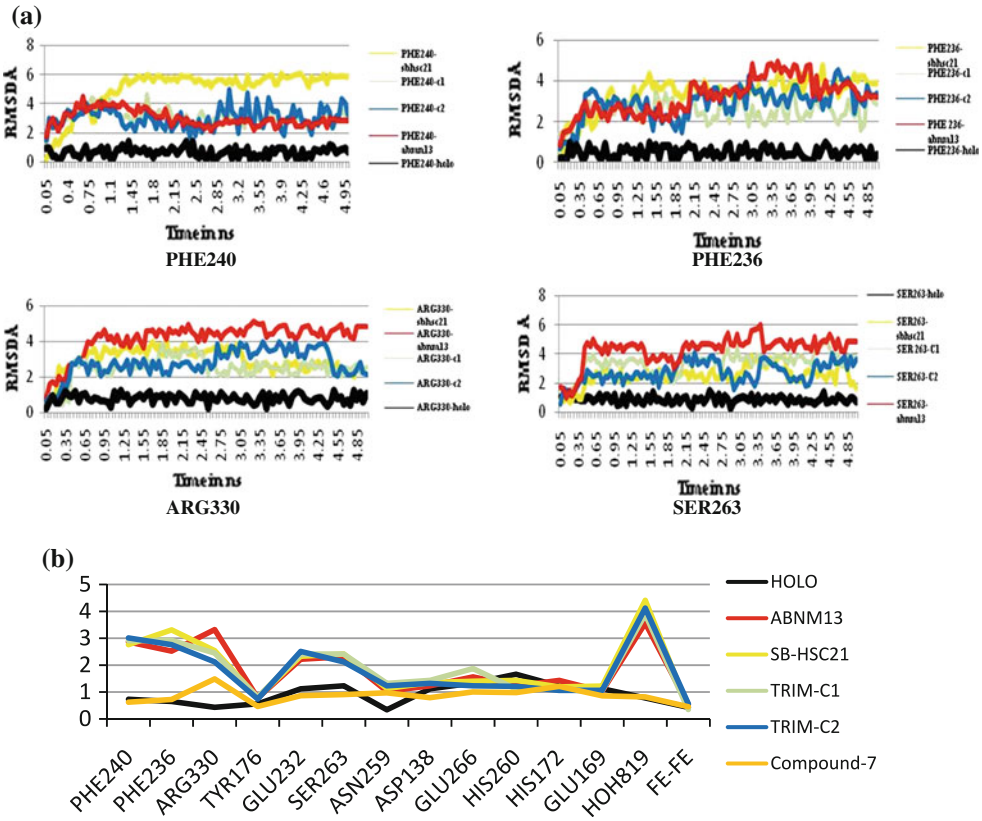

Fig. 13 **a** Comparison of movement of different key active site residues (PHE240, PHE236, SER263, ARG330) with different inhibitors, and the holo enzyme (without any inhibitor, *black lines*), ABNM13 (*red lines*), trimidox-c1, green lines, trimidox-c2, blue lines, SB-HSC21, *yellow lines*. **b** RMSF (root mean square fluctuations) values averaged over 5 ns of different residues, as compared with the holo enzyme

inhibitors were induced. We also observed a relatively low and erratic pattern during the binding energy calculations. The MD trajectory poses and estimated binding energy from eMBrAcE minimization are presented in Fig. 14a, b.

Conclusions

The study provided a clear perception about the active site of RR and the molecular recognition process of the three RR inhibitors SB-HSC21, ABNM13, and trimidox. We identified, the active site is closed by a water bridge between SER263 and GLU232. On approach of the incoming ligands this bridge is broken, and the residues move just enough to accommodate these ligands. The study provided the clues necessary to launch the first step towards developing a valid structure based model. We got the following clues, which are significant for future drug design on this target: (a) we got a definite proof that the active site is malleable and shows significant induced fit. (b) key residues were identified, which are responsible for ligand interactions (c) a remarkably stable H-bond with TYR176 hydroxyl oxygen and the –NHOH (Trimidox-Cluster1, SB-HSC21 and ABNM13 or phenolic –OH (Trimidox-Cluster2) were observed throughout the MD simulations (d) we identified a two stage gate keeping mechanism, first gate controlled by ARG330, and second gate controlled by SER263, PHE240,

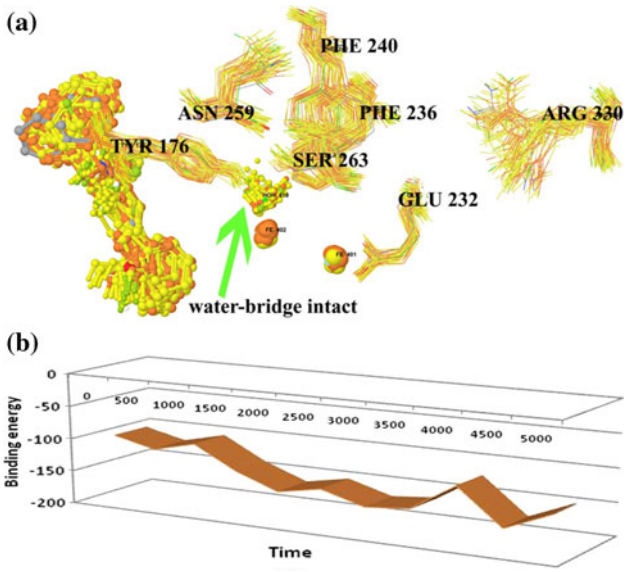

Fig. 14 **a** Superposition of trajectories at regular intervals for MD simulation of hRRM2 with compound 7. **b** Estimated binding energy for eMBrAcE minimization

and PHE236, and (e) for holo enzyme dynamics, active site aminoacid residues during MD simulation did not deviate significantly, neither we have observed the disruption of the water bridge.

Throughout the study we focused on searching for plausible interactions, which supports our hypothesis: The

inhibitors act by disrupting the water bridge between TYR176 oxygen and di-iron center thereby, ceasing the electron transfer. We also got important information on how amidoximes, hydroxamates, and phenolics may act as RR inhibitor. After the MD simulation we ended with a model, which is likely to mimic the biological system very closely. The developed model must be able to successfully screen any ligand dataset, and should produce good enrichment in any virtual screening (VS) validation experiment. Therefore, the study could have been extended to validation of VS on this particular target. For a VS validation experiment we need a set of actives (ligands) and inactives (decoys). However, very few molecules were reported to be a selective hRRM2 inhibitor. As more and more active molecules come up it would be possible to design specific actives/decoy dataset in future to setup a structure based VS experiment. The resulting structures after a 5 ns dynamics are available as Supplementary Material. Readers can use them for future structure based drug discovery, or VS experiment.

Acknowledgments We thank University Grants Commission for providing necessary financial support for the current work. We also thank Mrs. Nibha Mishra and Dr. Venkatesan J for proofreading our manuscript.

References

1. Shao J, Zhou B, Chu B, Yen Y (2006) Ribonucleotide reductase inhibitors and future drug design. Curr Cancer Drug Targets 6:409
2. Cerqueira NM, Pereira S, Fernandes PA, Ramos MJ (2005) Overview of ribonucleotide reductase inhibitors: an appealing target in anti-tumour therapy. Curr Med Chem 12:1283
3. Stubbe JA, Nocera DG, Yee CS, Chang MCY (2003) Radical initiation in the class I ribonucleotide reductase: long-range proton-coupled electron transfer? Chem Rev 103:2167
4. Stubbe JA, van der Donk WA (1998) Protein radicals in enzyme catalysis. Chem Rev 98:705
5. Jordan A, Reichard P (1998) Ribonucleotide reductases. Annu Rev Biochem 67:71
6. Reichard P (1993) From RNA to DNA, why so many ribonucleotide reductases? Science 260:1773
7. Reichard P, Ehrenberg A (1983) Ribonucleotide reductase—a radical enzyme. Science 221:514
8. Jordan A, Pontis E, Atta M, Krook M, Gibert I, Barbe J, Reichard P (1994) A second class I ribonucleotide reductase in enterobacteriaceae: characterization of the *Salmonella typhimurium* enzyme. Proc Natl Acad Sci USA 91:12892
9. Högbom M, Stenmark P, Voevodskaya N, McClarty G, Gräslund A, Nordlund P (2004) The radical site in chlamydial ribonucleotide reductase defines a new R2 subclass. Science 305:245
10. Smith BD, Karp JE (2003) Ribonucleotide reductase: an old target with new potential. Leuk Res 27:1075
11. Nocentini G (1996) Ribonucleotide reductase inhibitors: new strategies for cancer chemotherapy. Crit Rev Oncol Hematol 22:89
12. Holland KP, Elford HL, Bracchi V, Annis CG, Schuster SM, Chakrabarti D (1998) Antimalarial activities of polyhydroxyphenyl and hydroxamic acid derivatives. Antimicrob Agents Chemother 42:2456
13. Yun D, Saleh L, García-Serres R, Chicalese BM, An YH, Huynh BH, Bollinger JM Jr (2007) Addition of oxygen to the diiron (II/II) cluster is the slowest step in formation of the tyrosyl radical in the W103Y variant of ribonucleotide reductase protein R2 from mouse. Biochemistry 46:13067
14. Smith P, Zhou B, Ho N, Yuan YC, Su L, Tsai SC, Yen Y (2009) 2.6 Å X-ray crystal structure of human p53R2, a p53-inducible ribonucleotide reductase. Biochemistry 48:11134
15. Strand KR, Karlsen S, Kolberg M, Røhr ÅK, Görbitz CH, Andersson KK (2004) Crystal structural studies of changes in the native dinuclear iron center of ribonucleotide reductase protein R2 from mouse. J Biol Chem 279:46794
16. Logan DT, Su XD, Åberg A, Regnström K, Hajdu J, Eklund H, Nordlund P (1996) Crystal structure of reduced protein R2 of ribonucleotide reductase: the structural basis for oxygen activation at a dinuclear iron site. Structure 4:1053
17. Nordlund P, Sjöberg BM, Eklund H (1990) Three-dimensional structure of the free radical protein of ribonucleotide reductase. Nature 345:593
18. Nordlund P, Eklund H (1993) Structure and function of the *Escherichia coli* ribonucleotide reductase protein R2. J Mol Biol 232:123
19. Končić MZ, Barbarić M, Perković I, Zorc B (2011) Antiradical, chelating and antioxidant activities of hydroxamic acids and hydroxyureas. Molecules 16:6232
20. Fritzer-Szekeres M, Grusch M, Luxbacher C, Horvath S, Krupitza G, Elford HL, Szekeres T (2000) Trimidox, an inhibitor of ribonucleotide reductase, induces apoptosis and activates caspases in HL-60 promyelocytic leukemia cells. Exp Hematol 28:924
21. Ren S, Wang R, Komatsu K, Bonaz-Krause P, Zyrianov Y, McKenna CE, Csipke C, Tokes ZA, Lien EJ (2002) Synthesis, biological evaluation, and quantitative structure-activity relationship analysis of new Schiff bases of hydroxysemicarbazide as potential antitumor agents. J Med Chem 45:410
22. Shao J, Zhou B, Zhu L, Bilio AJ, Su L, Yuan YC, Ren S, Lien EJ, Shih J, Yen Y (2005) Determination of the potency and subunit-selectivity of ribonucleotide reductase inhibitors with a recombinant-holoenzyme-based in vitro assay. Biochem Pharmacol 69:627
23. Elford HL (1994) assignee. Method of treating hemoglobinopathies. US Patent 5,366,996
24. Basu A, Sinha BN, Saiko P, Graser G, Szekeres T (2011) *N*-hydroxy-*N*′-aminoguanidines as anti-cancer lead molecule: QSAR, synthesis and biological evaluation. Bioorg Med Chem Lett 21:3324
25. Saiko P, Graser G, Giessrigl B, Lackner A, Grusch M, Krupitza G, Basu A, Sinha B, Jayaprakash V, Jaeger W (2011) A novel *N*-hydroxy-*N*′-aminoguanidine derivative inhibits ribonucleotide reductase activity: effects in human HL-60 promyelocytic leukemia cells and synergism with arabinofuranosylcytosine (Ara-C). Biochem Pharmacol 81:50
26. Krishnan K, Prathiba K, Jayaprakash V, Basu A, Mishra N, Zhou B, Hu S, Yen Y (2008) Synthesis and ribonucleotide reductase inhibitory activity of thiosemicarbazones. Bioorg Med Chem Lett 18:6248
27. Himo F, Siegbahn PEM (2003) Quantum chemical studies of radical-containing enzymes. Chem Rev 103:2421
28. Torrent M, Musaev DG, Basch H, Morokuma K (2002) Computational studies of reaction mechanisms of methane monooxygenase and ribonucleotide reductase. J Comput Chem 23:59
29. Lynch J, Juarez-Garcia C, Münck E, Que L Jr (1989) Mössbauer and EPR studies of the binuclear iron center in ribonucleotide reductase from *Escherichia coli*. a new iron-to-protein stoichiometry. J Biol Chem 264:8091

30. Elgren TE, Hendrich MP, Que L Jr (1993) Azide binding to the diferrous clusters of the R2 protein of ribonucleotide reductase from *Escherichia coli*. J Am Chem Soc 115:9291
31. Bell CL, Nambury C, Bauer L (1964) The structure of amidoximes. J Org Chem 29:2873
32. Kjøller Larsen I, Sjöoberg BM, Thelander L (1982) Characterization of the active site of ribonucleotide reductase of *Escherichia coli*, bacteriophage T4 and mammalian cells by inhibition studies with hydroxyurea analogues. Eur J Biochem 125:75